Cite as: X. Zhao *et al.*, *Science* 10.1126/science.abn5679 (2022).

Accelerated aging of all-inorganic, interface-stabilized perovskite solar cells

Xiaoming Zhao[1], Tianran Liu[1,2], Quinn C. Burlingame[3], Tianjun Liu[4], Rudolph Holley III[1], Guangming Cheng[5], Nan Yao[5], Feng Gao[4], Yueh-Lin Loo[1]*

[1]Department of Chemical and Biological Engineering, Princeton University, Princeton, NJ 08544, USA. [2]Department of Electrical and Computer Engineering, Princeton University, Princeton, NJ 08544, USA. [3]Andlinger Center for Energy and the Environment, Princeton University, Princeton, NJ 08544, USA. [4]Department of Physics, Chemistry, and Biology (IFM), Linköping University, Linköping, SE-58183, Sweden. [5]Princeton Institute for the Science and Technology of Materials, Princeton University, Princeton, NJ 08544, USA.

*Corresponding author. Email: lloo@princeton.edu

To understand degradation routes and improve the stability of perovskite solar cells (PSCs), accelerated aging tests are needed. Here, we use elevated temperatures (up to 110 Celsius) to quantify the accelerated degradation of encapsulated $CsPbI_3$ PSCs under constant illumination. Incorporating a 2D $Cs_2PbI_2Cl_2$ capping layer between the perovskite active layer and hole-transport layer stabilizes the interface while increasing power conversion efficiency of the all-inorganic PSCs from 14.9% to 17.4%. Devices with this 2D capping layer did not degrade at 35 Celsius and required >2100 hours at 110 Celsius under constant illumination to degrade by 20% of their initial efficiency. Degradation acceleration factors based on the observed Arrhenius temperature dependence predict intrinsic lifetimes of 51,000 ± 7,000 hours (>5 years) operating continuously at 35 Celsius.

Although the power-conversion efficiencies (PCEs) of metal halide perovskite solar cells (PSCs) can now exceed 25%, long-term operational instability issues must be addressed before they can be commercialized (*1*–*3*). The most stable and efficient PSCs have reported T_{80} lifetimes (the time at which the PCE drops to 80% of its initial value) of just a few hundred or thousand hours (*4*–*7*) under continuous illumination, versus the >20 year lifetimes required for most commercial applications. While there is an encouraging report of PSCs with a T_{80} of more than one year, the PCE of the solar cells is relatively low (<13%) (*8*). Accelerated aging tests can facilitate rapid PSC stability screening (*9*–*11*). An effective accelerated stress test can quantify the lifetime acceleration factor (AF) that relates the lifetime under a defined standard operating condition to the lifetime under elevated stress conditions. Thermal and high-intensity illumination stress tests with AFs have been developed for organic- and silicon-based PVs (*11*–*15*), but developing robust AFs for PSCs is challenging given their complex sensitivities to temperature, light, and electrical bias (*10*, *16*, *17*).

Here, we thermally accelerated the degradation of encapsulated $CsPbI_3$ PSCs operating under constant illumination at their maximum power point (MPP) with temperatures from 35° to 110°C. The PCE degradation rate followed an Arrhenius temperature dependence that was slowed substantially by incorporating a 2D $Cs_2PbI_2Cl_2$ capping layer between the perovskite active layer and the hole transport layer (HTL). This 2D layer stabilized the perovskite/HTL interface and suppressed ion migration into the HTL, resulting in a T_{80} lifetime of > 2100 hours at 110°C. With an experimentally determined AF of 24.2 ± 3.5, this lifetime corresponds to an extrapolated T_{80} of 5.1 ± 0.7 × 10^4 hours—or more than 5 yr of continuous operation at 35°C.

The most efficient PSCs have been based on hybrid organic-inorganic perovskites, which contain volatile organic cations, such as methylammonium (MA^+) and formamidinium (FA^+). To maximize the thermal and photostability of our solar cells, we chose inorganic $CsPbI_3$ as the photo-absorber (*18*–*20*), despite its solar cells exhibiting slightly lower efficiencies. Inorganic $CsPbI_3$ PSCs with the structure shown in Fig. 1A were fabricated both with (capped) and without (uncapped) a 2D $Cs_2PbI_2Cl_2$ layer between the $CsPbI_3$ absorber and the CuSCN HTL. The all-inorganic stack that includes TiO_2, Al_2O_3, and CuSCN transport layers as well as fluorinated tin oxide (FTO) and Cr/Au electrodes was designed to maximize the thermal and photostability of these devices, as discussed in supplementary text 1 and fig. S1. Photovoltaic characterization of representative as-fabricated devices are shown in Fig. 1, B and C, fig. S2, and listed in table S1; with population statistics as shown in fig. S3. Capped PSCs have improved fill factors (FF's) and open-circuit voltages (V_{OC}'s), leading to a champion PCE of 17.4% compared with 14.9% for uncapped devices. This PCE is the highest among fully-inorganic PSCs in which all the functional materials in the stack are inorganic.

Depositing a thin 2D perovskite capping layer can stabilize the surfaces of organic-inorganic hybrid perovskites, such as $FAPbI_3$ and $MAPbI_3$ (*21*), but this approach has not yet

been successfully implemented with inorganic perovskites. This challenge stems from the stronger binding strength of Cs^+ compared to MA^+ or FA^+, which prevents cation exchange between the Cs^+ of $CsPbI_3$ and the organic ligands in the applied hybrid organic/inorganic 2D perovskite precursor solution (*22*–*25*). To avoid this problem, we deposited a fully inorganic $Cs_2PbI_2Cl_2$ 2D layer by treating the $CsPbI_3$ surface with a CsCl solution followed by thermally annealing. Grazing-incidence wide-angle x-ray scattering (GIWAXS) patterns (Fig. 2A and fig. S4) showed two new reflections emerging on $CsPbI_3$ films after CsCl treatment corresponding to the (002) and (004) reflections of 2D $Cs_2PbI_2Cl_2$. Increasing the incident angle of the x-ray beam resulted a decrease in the relative intensity of these reflections (Fig. 2B), suggesting that the 2D layer formed preferentially on the $CsPbI_3$ surface. The interfacial nature of this 2D layer was also confirmed by cross-sectional scanning electron microscopy (SEM) imaging of the device (fig. S5). We estimated the thickness of the capping layer to be 20 nm by tracking chlorine content on the film surface with x-ray photoelectron spectroscopy (XPS) while depth etching (Fig. 2C).

To study the surface passivation effect of this capping layer, we measured time-resolved photoluminescence (TRPL) transients (Fig. 2D). The lifetime of the device increased from 14 ns to >62 ns in the presence of the capping layer, suggesting that it effectively suppressed non-radiative recombination at the $CsPbI_3$ surface and extended the lifetime and diffusion length of charge carriers (*26*). This observation is consistent with the observed V_{OC} increase in capped PSCs, (Fig. 1B), and whose PV characteristics are tabulated in table S1. This trend was also comparable to previous reports of 2D/3D PSCs based on organic-inorganic hybrid perovskites that benefited from surface passivation (*26*–*28*).

To evaluate the stability of capped and uncapped PSCs, N_2-encapsulated solar cells (fig. S6) with both structures were aged at their maximum power point (MPP) under illumination from a metal halide solar simulator (spectrum shown in fig. S7) at 35°, 59°, 85°, and 110°C. Our stability studies employed solar cells having the same device configuration as those for PV characterization, including encapsulation and the light aperture. The evolution of the normalized PCE (averaged from 3 subcells) for both device types at these operating temperatures, and the evolution for the unnormalized data, normalized short-circuit current (J_{SC}), V_{OC}, FF, and EQE is shown in figs. S8 to S10. Figure S11 shows the operational stability of 2D/3D PSCs without encapsulation operating at 110°C, confirming the robustness of our solar cell packaging. Heating the solar cells reversibly reduced their PCEs (*29*), which accounts for the differences in the initial PCE of the un-normalized data set in fig. S8. We observe a clear temperature dependence of the PCE degradation rate that can be fitted to a bi-exponential function of the form:

$$PCE(t) = A1^{*}\exp\left(-k_{fast}\times t\right) + A2^{*}\exp\left(-k_{slow}\times t\right) + B \quad (1)$$

with a fast and slow degradation rate, k_{fast} and k_{slow}. Here, *A1*, *A2* and *B* are constants and *t* is time. We fit the data collected across the temperature range using this function with an $R^2 > 0.95$, except for the data acquired on the capped solar cells operating at 35°C because no PCE degradation was observed, even after 3531 hr of continuous operation (Fig. 3B).

To estimate an activation energy for the degradation processes corresponding to k_{fast} and k_{slow}, we assume an Arrhenius temperature dependence to the degradation rates:

$$k(T) = A\exp\left(\frac{-E_a}{k_B T}\right) \quad (2)$$

where $k(T)$ is a degradation rate at temperature T, A is constant, E_a is the activation energy of degradation, and k_B is Boltzmann's constant (*11*–*15*). Rearranging *Eq. (2)*, the activation energy is equivalent to the slope:

$$E_a = -\frac{\partial \ln\left(k(T)\right)}{\partial\left(\frac{1}{k_B T}\right)} \quad (3)$$

The temperature-dependent degradation rates were plotted as a function of inverse temperature in Fig. 3C and fitted to *Eq. (3)*. Degradation rates could be adequately described by a single Arrhenius function across the entire temperature range. This finding suggested that the same degradation mechanism dominated the entire temperature range, which is an important criteria for a reliable accelerated aging test (*9*). We observed that the activation energies associated with the fast and slow degradation of each type of PSC were comparable, suggesting that the two degradation rates probed a single physical process. As we will discuss in detail below, we speculate that ion migration is the dominant degradation mechanism. The E_a that describe the degradation for capped PSCs are nearly twice those for uncapped PSCs, suggesting that the 2D $Cs_2PbI_2Cl_2$ layer stabilizes the devices against thermal degradation stemming from ion migration.

To extract a meaningful degradation rate at standard operating conditions, k_{ref}, from the accelerated degradation rate at high temperatures, k_{acc}, we define an AF (*11*):

$$AF = \frac{k_{acc}}{k_{ref}} = \exp\left(\frac{E_a}{k_B}\left[\frac{1}{T_{ref}} - \frac{1}{T_{acc}}\right]\right) \quad (4)$$

where T_{acc} and T_{ref} are the operating temperatures during aging at accelerated and standard operating conditions (defined as 1 sun intensity, 35°C). Because k_{slow} is primarily responsible for long-term degradation and the E_as of the two rates are nearly identical, we used the E_a extracted from k_{slow} and *Eq. (4)* to obtain AFs for each T_{acc} (specifically 59°, 85°, and 110°C) (Fig. 3D). Based on these AFs, we can define an equivalent operating time at T_{ref} = 35°C for devices aged at elevated temperatures by multiplying their aging time by the

acceleration factor (Fig. 3, E and F). When processed in this manner, all of the data collapsed onto a universal curve for both capped and uncapped solar cells, which further confirmed that the same mechanism, albeit hastened at elevated temperatures, was responsible for degradation across the entire temperature range. With this data set, we can make T_{80} lifetime predictions for capped devices operating at 35°C. This estimate is critical since devices aged at these conditions do not show any PCE degradation, even after continuous operation for 3531 hr. Given that the average experimentally measured T_{80} for capped solar cells operating continuously at 110°C is 2100 hours (Fig. 3B), and the AF for the capped solar cells at 110°C is 24.2 ± 3.5, we estimated a T_{80} of 5.1 ± 0.7 × 10^4 hr at 35°C.

In order to investigate the origins of PSC degradation, we aged full-stack devices at 110°C under continuous illumination before peeling off their top electrodes and characterizing the structure of the active layers with x-ray diffraction (XRD). As shown in Fig. 4, A and B, the reflection at 2θ = 16.15° corresponding to the (003) reflection of CuSCN in the XRD trace of the uncapped PSCs became broader and less intense after 2000 hours of aging, which suggested a decrease in the CuSCN crystallite size. Clear degradation of the CuSCN surface in aged, uncapped PSCs was also visible in the SEM images in fig. S12, which show the formation of pinholes and decreased film uniformity. Correspondingly, the I 3d signal increased substantially in the XPS spectrum of the aged HTL surface (Fig. 4C). These results suggest that iodine migration from the $CsPbI_3$ active layer was responsible for the structural changes in CuSCN in uncapped solar cells, as discussed in supplementary text 2 and figs. S13 and S14. In contrast, the film structure and morphology of CuSCN in capped PSCs did not show appreciable changes after the same duration, as shown in their XRD patterns and SEM images (Fig. 4, A and B, and fig. S12), and we did not observe any appreciable I 3d signal in the XPS spectrum of the HTL surface of capped PSCs (Fig. 4C).

To quantify the ease of ion migration in capped and uncapped films, we measured the temperature-dependent conductivity in two-terminal lateral devices, a widely used method for characterizing ion migration in perovskite films (*4*, *30*, *31*). The activation energy of ion migration ($E_{a,ion}$) values were extracted by fitting the measured temperature-dependent conductivity (σ) to the Nernst-Einstein equation,

$$\sigma(T) = \frac{\sigma_0}{T}\exp\left(\frac{-E_{a,ion}}{k_B T}\right) \quad (5)$$

where σ_0 is a temperature-independent pre-factor (*30*, *31*). Plotting 1/T vs. ln(σT), two distinct regions were present in both capped and uncapped films corresponding to two distinct transport regimes. The high-temperature linear regime, corresponding to ion-dominated transport, was used to extract an approximate $E_{a,ion}$ (Fig. 4D). Similar to the activation of degradation, the $E_{a,ion}$ of the capped film is nearly twice that of the uncapped film indicating that the 2D cap frustrated ion migration. Suppressed ion migration likely stems from passivation of iodine vacancies at the surface of the perovskite active layer in the presence of a 2D capping layer (*4, 32, 33*), as shown in fig. S15.

REFERENCES AND NOTES

1. M. Grätzel, The light and shade of perovskite solar cells. *Nat. Mater.* **13**, 838–842 (2014). doi:10.1038/nmat4065 Medline
2. N. Li, X. Niu, Q. Chen, H. Zhou, Towards commercialization: The operational stability of perovskite solar cells. *Chem. Soc. Rev.* **49**, 8235–8286 (2020). doi:10.1039/D0CS00573H Medline
3. H. Min, D. Y. Lee, J. Kim, G. Kim, K. S. Lee, J. Kim, M. J. Paik, Y. K. Kim, K. S. Kim, M. G. Kim, T. J. Shin, S. Il Seok, Perovskite solar cells with atomically coherent interlayers on SnO_2 electrodes. *Nature* **598**, 444–450 (2021). doi:10.1038/s41586-021-03964-8 Medline
4. S. Yang, S. Chen, E. Mosconi, Y. Fang, X. Xiao, C. Wang, Y. Zhou, Z. Yu, J. Zhao, Y. Gao, F. De Angelis, J. Huang, Stabilizing halide perovskite surfaces for solar cell operation with wide-bandgap lead oxysalts. *Science* **365**, 473–478 (2019). doi:10.1126/science.aax3294 Medline
5. Z. Dai, S. K. Yadavalli, M. Chen, A. Abbaspourtamijani, Y. Qi, N. P. Padture, Interfacial toughening with self-assembled monolayers enhances perovskite solar cell reliability. *Science* **372**, 618–622 (2021). doi:10.1126/science.abf5602 Medline
6. N. Arora, M. I. Dar, A. Hinderhofer, N. Pellet, F. Schreiber, S. M. Zakeeruddin, M. Grätzel, Perovskite solar cells with CuSCN hole extraction layers yield stabilized efficiencies greater than 20. *Science* **358**, 768–771 (2017). doi:10.1126/science.aam5655 Medline
7. Y. H. Lin, N. Sakai, P. Da, J. Wu, H. C. Sansom, A. J. Ramadan, S. Mahesh, J. Liu, R. D. J. Oliver, J. Lim, L. Aspitarte, K. Sharma, P. K. Madhu, A. B. Morales-Vilches, P. K. Nayak, S. Bai, F. Gao, C. R. M. Grovenor, M. B. Johnston, J. G. Labram, J. R. Durrant, J. M. Ball, B. Wenger, B. Stannowski, H. J. Snaith, A piperidinium salt stabilizes efficient metal-halide perovskite solar cells. *Science* **369**, 96–102 (2020). doi:10.1126/science.aba1628 Medline
8. G. Grancini, C. Roldán-Carmona, I. Zimmermann, E. Mosconi, X. Lee, D. Martineau, S. Narbey, F. Oswald, F. De Angelis, M. Graetzel, M. K. Nazeeruddin, One-Year stable perovskite solar cells by 2D/3D interface engineering. *Nat. Commun.* **8**, 15684 (2017). doi:10.1038/ncomms15684 Medline
9. M. V. Khenkin, E. A. Katz, A. Abate, G. Bardizza, J. J. Berry, C. Brabec, F. Brunetti, V. Bulović, Q. Burlingame, A. Di Carlo, R. Cheacharoen, Y.-B. Cheng, A. Colsmann, S. Cros, K. Domanski, M. Dusza, C. J. Fell, S. R. Forrest, Y. Galagan, D. Di Girolamo, M. Grätzel, A. Hagfeldt, E. von Hauff, H. Hoppe, J. Kettle, H. Köbler, M. S. Leite, S. Liu, Y.-L. Loo, J. M. Luther, C.-Q. Ma, M. Madsen, M. Manceau, M. Matheron, M. McGehee, R. Meitzner, M. K. Nazeeruddin, A. F. Nogueira, Ç. Odabaşı, A. Osherov, N.-G. Park, M. O. Reese, F. De Rossi, M. Saliba, U. S. Schubert, H. J. Snaith, S. D. Stranks, W. Tress, P. A. Troshin, V. Turkovic, S. Veenstra, I. Visoly-Fisher, A. Walsh, T. Watson, H. Xie, R. Yıldırım, S. M. Zakeeruddin, K. Zhu, M. Lira-Cantu, Consensus statement for stability assessment and reporting for perovskite photovoltaics based on ISOS procedures. *Nat. Energy* **5**, 35–49 (2020). doi:10.1038/s41560-019-0529-5
10. K. M. Anoop, M. V. Khenkin, F. Di Giacomo, Y. Galagan, S. Rahmany, L. Etgar, E. A. Katz, I. Visoly-Fisher, Bias-Dependent Stability of Perovskite Solar Cells Studied Using Natural and Concentrated Sunlight. *Sol. RRL* **4**, 1900335 (2020). doi:10.1002/solr.201900335
11. O. Haillant, D. Dumbleton, A. Zielnik, An Arrhenius approach to estimating organic photovoltaic module weathering acceleration factors. *Sol. Energy Mater. Sol. Cells* **95**, 1889–1895 (2011). doi:10.1016/j.solmat.2011.02.013
12. J. Kettle, V. Stoichkov, D. Kumar, M. Corazza, S. A. Gevorgyan, F. C. Krebs, Using ISOS consensus test protocols for development of quantitative life test models in ageing of organic solar cells. *Sol. Energy Mater. Sol. Cells* **167**, 53–59 (2017). doi:10.1016/j.solmat.2017.04.005
13. Q. Burlingame, B. Song, L. Ciammaruchi, G. Zanotti, J. Hankett, Z. Chen, E. A. Katz, S. R. Forrest, Reliability of Small Molecule Organic Photovoltaics with Electron-

Filtering Compound Buffer Layers. *Adv. Energy Mater.* **6**, 1601094 (2016). doi:10.1002/aenm.201601094
14. S. Züfle, R. Hansson, E. A. Katz, E. Moons, Initial photo-degradation of PCDTBT:PC70BM solar cells studied under various illumination conditions: Role of the hole transport layer. *Sol. Energy* **183**, 234–239 (2019). doi:10.1016/j.solener.2019.03.020
15. Q. Burlingame, X. Huang, X. Liu, C. Jeong, C. Coburn, S. R. Forrest, Intrinsically stable organic solar cells under high-intensity illumination. *Nature* **573**, 394–397 (2019). doi:10.1038/s41586-019-1544-1 Medline
16. Z. Wang, Q. Lin, B. Wenger, M. G. Christoforo, Y. H. Lin, M. T. Klug, M. B. Johnston, L. M. Herz, H. J. Snaith, High irradiance performance of metal halide perovskites for concentrator photovoltaics. *Nat. Energy* **3**, 855–861 (2018). doi:10.1038/s41560-018-0220-2
17. C. Law, L. Miseikis, S. Dimitrov, P. Shakya-Tuladhar, X. Li, P. R. F. Barnes, J. Durrant, B. C. O'Regan, Performance and stability of lead perovskite/TiO2, polymer/PCBM, and dye sensitized solar cells at light intensities up to 70 suns. *Adv. Mater.* **26**, 6268–6273 (2014). doi:10.1002/adma.201402612 Medline
18. S. M. Yoon, H. Min, J. B. Kim, G. Kim, K. S. Lee, S. Il Seok, Surface Engineering of Ambient-Air-Processed Cesium Lead Triiodide Layers for Efficient Solar Cells. *Joule* **5**, 183–196 (2021). doi:10.1016/j.joule.2020.11.020
19. Y. Wang, X. Liu, T. Zhang, X. Wang, M. Kan, J. Shi, Y. Zhao, The Role of Dimethylammonium Iodide in $CsPbI_3$ Perovskite Fabrication: Additive or Dopant? *Angew. Chem. Int. Ed.* **58**, 16691–16696 (2019). doi:10.1002/anie.201910800 Medline
20. Y. Wang, M. I. Dar, L. K. Ono, T. Zhang, M. Kan, Y. Li, L. Zhang, X. Wang, Y. Yang, X. Gao, Y. Qi, M. Grätzel, Y. Zhao, Thermodynamically stabilized β-$CsPbI_3$-based perovskite solar cells with efficiencies >18. *Science* **365**, 591–595 (2019). doi:10.1126/science.aav8680 Medline
21. D. L. McGott, C. P. Muzzillo, C. L. Perkins, J. J. Berry, K. Zhu, J. N. Duenow, E. Colegrove, C. A. Wolden, M. O. Reese, 3D/2D passivation as a secret to success for polycrystalline thin-film solar cells. *Joule* **5**, 1057–1073 (2021). doi:10.1016/j.joule.2021.03.015
22. X. Liu, X. Wang, T. Zhang, Y. Miao, Z. Qin, Y. Chen, Y. Zhao, Organic Tetrabutylammonium Cation Intercalation to Heal Inorganic $CsPbI_3$ Perovskite. *Angew. Chem. Int. Ed.* **60**, 12351–12355 (2021). doi:10.1002/anie.202102538 Medline
23. Y. Wang, T. Zhang, M. Kan, Y. Li, T. Wang, Y. Zhao, Efficient α-CsPbI3 Photovoltaics with Surface Terminated Organic Cations. *Joule* **2**, 2065–2075 (2018). doi:10.1016/j.joule.2018.06.013
24. E. M. Sanehira, A. R. Marshall, J. A. Christians, S. P. Harvey, P. N. Ciesielski, L. M. Wheeler, P. Schulz, L. Y. Lin, M. C. Beard, J. M. Luther, Enhanced mobility $CsPbI_3$ quantum dot arrays for record-efficiency, high-voltage photovoltaic cells. *Sci. Adv.* **3**, eaao4204 (2017). doi:10.1126/sciadv.aao4204 Medline
25. Y. Wang, T. Zhang, M. Kan, Y. Zhao, Bifunctional Stabilization of All-Inorganic α-$CsPbI_3$ Perovskite for 17% Efficiency Photovoltaics. *J. Am. Chem. Soc.* **140**, 12345–12348 (2018). doi:10.1021/jacs.8b07927 Medline
26. Q. Jiang, Y. Zhao, X. Zhang, X. Yang, Y. Chen, Z. Chu, Q. Ye, X. Li, Z. Yin, J. You, Surface passivation of perovskite film for efficient solar cells. *Nat. Photonics* **13**, 460–466 (2019). doi:10.1038/s41566-019-0398-2
27. X. Jiang, S. Chen, Y. Li, L. Zhang, N. Shen, G. Zhang, J. Du, N. Fu, B. Xu, Direct Surface Passivation of Perovskite Film by 4-Fluorophenethylammonium Iodide toward Stable and Efficient Perovskite Solar Cells. *ACS Appl. Mater. Interfaces* **13**, 2558–2565 (2021). doi:10.1021/acsami.0c17773 Medline
28. W. Shi, H. Ye, Efficient and Stable Perovskite Solar Cells with a Superhydrophobic Two-Dimensional Capping Layer. *J. Phys. Chem. Lett.* **12**, 4052–4058 (2021). doi:10.1021/acs.jpclett.1c01036 Medline
29. T. Moot, J. B. Patel, G. McAndrews, E. J. Wolf, D. Morales, I. E. Gould, B. A. Rosales, C. C. Boyd, L. M. Wheeler, P. A. Parilla, S. W. Johnston, L. T. Schelhas, M. D. McGehee, J. M. Luther, Temperature Coefficients of Perovskite Photovoltaics for Energy Yield Calculations. *ACS Energy Lett.* **6**, 2038–2047 (2021). doi:10.1021/acsenergylett.1c00748
30. J. Xing, Q. Wang, Q. Dong, Y. Yuan, Y. Fang, J. Huang, Ultrafast ion migration in hybrid perovskite polycrystalline thin films under light and suppression in single crystals. *Phys. Chem. Chem. Phys.* **18**, 30484–30490 (2016). doi:10.1039/C6CP06496E Medline
31. X. Li, W. Zhang, Y. C. Wang, W. Zhang, H. Q. Wang, J. Fang, In-situ cross-linking strategy for efficient and operationally stable methylammoniun lead iodide solar cells. *Nat. Commun.* **9**, 3806 (2018). doi:10.1038/s41467-018-06204-2 Medline
32. B. Chen, P. N. Rudd, S. Yang, Y. Yuan, J. Huang, Imperfections and their passivation in halide perovskite solar cells. *Chem. Soc. Rev.* **48**, 3842–3867 (2019). doi:10.1039/C8CS00853A Medline
33. X. Zhao, T. Liu, Y.-L. Loo, Advancing 2D Perovskites for Efficient and Stable Solar Cells: Challenges and Opportunities. *Adv. Mater.* **34**, e2105849 (2022). doi:10.1002/adma.202105849 Medline
34. B.-B. Zhang, B. Xiao, S. Dong, Y. Xu, The preparation and characterization of quasi-one-dimensional lead based perovskite CsPbI3 crystals from HI aqueous solutions. *J. Cryst. Growth* **498**, 1–4 (2018). doi:10.1016/j.jcrysgro.2018.05.027
35. P. Yang, S. Ullah, J. Wang, L. Liu, S. E. Yang, T. Xia, H. Guo, Y. Chen, Improving the phase stability of CsPbI3nanocrystalline films via polyvinylpyrrolidone additive engineering for photodetector application. *J. Phys. D Appl. Phys.* **54**, 205501 (2021). doi:10.1088/1361-6463/abe3b2
36. K. S. Shamala, L. C. S. Murthy, K. N. Rao, Studies on optical and dielectric properties of Al2O 3 thin films prepared by electron beam evaporation and spray pyrolysis method. *Mater. Sci. Eng. B Solid-State Mater. Adv. Technol.* **106**, 269–274 (2004).
37. J. Zhao, Y. Deng, H. Wei, X. Zheng, Z. Yu, Y. Shao, J. E. Shield, J. Huang, Strained hybrid perovskite thin films and their impact on the intrinsic stability of perovskite solar cells. *Sci. Adv.* **3**, eaao5616 (2017). doi:10.1126/sciadv.aao5616 Medline
38. Y. Yuan, J. Chae, Y. Shao, Q. Wang, Z. Xiao, A. Centrone, J. Huang, Photovoltaic Switching Mechanism in Lateral Structure Hybrid Perovskite Solar Cells. *Adv. Energy Mater.* **5**, 1500615 (2015). doi:10.1002/aenm.201500615
39. C. R. Osterwald, Translation of device performance measurements to reference conditions. *Sol. Cells* **18**, 269–279 (1986). doi:10.1016/0379-6787(86)90126-2
40. V. Shrotriya, G. Li, Y. Yao, T. Moriarty, K. Emery, Y. Yang, Accurate measurement and characterization of organic solar cells. *Adv. Funct. Mater.* **16**, 2016–2023 (2006). doi:10.1002/adfm.200600489
41. Y. Du, H. Cai, Z. Xing, Y. Wu, J. Xu, Z. Li, L. Huang, J. Ni, J. Li, J. Zhang, Propelling efficiency and stability of planar perovskite solar cells via Al2O3 interface modification to compact TiO2 layer. *Org. Electron.* **51**, 249–256 (2017). doi:10.1016/j.orgel.2017.08.027
42. Y. N. Zhang, B. Li, L. Y. Zhang, L. W. Yin, Efficient electron transfer layer based on Al2O3 passivated TiO2 nanorod arrays for high performance evaporation-route deposited FAPbI3 perovskite solar cells. *Sol. Energy Mater. Sol. Cells* **170**, 187–196 (2017). doi:10.1016/j.solmat.2017.05.072
43. T. Ye, B. Zhou, F. Zhan, F. Yuan, S. Ramakrishna, D. Golberg, X. Wang, Below 200 °C Fabrication Strategy of Black-Phase CsPbI3 Film for Ambient-Air-Stable Solar Cells. *Sol. RRL* **4**, 2000014 (2020). doi:10.1002/solr.202000014
44. B. Li, Y. Zhang, L. Fu, T. Yu, S. Zhou, L. Zhang, L. Yin, Surface passivation engineering strategy to fully-inorganic cubic $CsPbI_3$ perovskites for high-performance solar cells. *Nat. Commun.* **9**, 1076 (2018). doi:10.1038/s41467-018-03169-0 Medline
45. B. Li, Y. Zhang, L. Fu, L. Zhang, Z. Liu, L. Yin, Two-dimensional black phosphorous induced exciton dissociation efficiency enhancement for high-performance all-inorganic CsPbI3 perovskite photovoltaics. *J. Mater. Chem. A Mater. Energy Sustain.* **7**, 22539–22549 (2019). doi:10.1039/C9TA06016B
46. F. Matebese, R. Taziwa, D. Mutukwa, Progress on the synthesis and application of CuSCN inorganic hole transport material in perovskite solar cells. *Materials* **11**, 2592 (2018). doi:10.3390/ma11122592 Medline
47. K. Domanski, J. P. Correa-Baena, N. Mine, M. K. Nazeeruddin, A. Abate, M. Saliba, W. Tress, A. Hagfeldt, M. Grätzel, Not All That Glitters Is Gold: Metal-Migration-Induced Degradation in Perovskite Solar Cells. *ACS Nano* **10**, 6306–6314 (2016). doi:10.1021/acsnano.6b02613 Medline
48. R. A. Kerner, S. Heo, K. Roh, K. MacMillan, B. W. Larson, B. P. Rand, Organic Hole Transport Material Ionization Potential Dictates Diffusion Kinetics of Iodine Species in Halide Perovskite Devices. *ACS Energy Lett.* **6**, 501–508 (2021). doi:10.1021/acsenergylett.0c02495
49. J. Carrillo, A. Guerrero, S. Rahimnejad, O. Almora, I. Zarazua, E. Mas-Marza, J. Bisquert, G. Garcia-Belmonte, Ionic Reactivity at Contacts and Aging of Methylammonium Lead Triiodide Perovskite Solar Cells. *Adv. Energy Mater.* **6**, 1502246 (2016). doi:10.1002/aenm.201502246

50. D. Wei, F. Ma, R. Wang, S. Dou, P. Cui, H. Huang, J. Ji, E. Jia, X. Jia, S. Sajid, A. M. Elseman, L. Chu, Y. Li, B. Jiang, J. Qiao, Y. Yuan, M. Li, Ion-Migration Inhibition by the Cation-π Interaction in Perovskite Materials for Efficient and Stable Perovskite Solar Cells. *Adv. Mater.* **30**, e1707583 (2018). doi:10.1002/adma.201707583 Medline
51. W. Zhang, S. Pathak, N. Sakai, T. Stergiopoulos, P. K. Nayak, N. K. Noel, A. A. Haghighirad, V. M. Burlakov, D. W. deQuilettes, A. Sadhanala, W. Li, L. Wang, D. S. Ginger, R. H. Friend, H. J. Snaith, Enhanced optoelectronic quality of perovskite thin films with hypophosphorous acid for planar heterojunction solar cells. *Nat. Commun.* **6**, 10030 (2015). doi:10.1038/ncomms10030 Medline
52. T. Wu, Y. Wang, X. Li, Y. Wu, X. Meng, D. Cui, X. Yang, L. Han, Efficient Defect Passivation for Perovskite Solar Cells by Controlling the Electron Density Distribution of Donor-π-Acceptor Molecules. *Adv. Energy Mater.* **9**, 1803766 (2019). doi:10.1002/aenm.201803766
53. X. Zhao, C. Yao, K. Gu, T. Liu, Y. Xia, Y.-L. Loo, A hole-transport material that also passivates perovskite surface defects for solar cells with improved efficiency and stability. *Energy Environ. Sci.* **13**, 4334–4343 (2020). doi:10.1039/D0EE01655A
54. S. P. Dunfield, L. Bliss, F. Zhang, J. M. Luther, K. Zhu, M. F. A. M. Hest, M. O. Reese, J. J. Berry, From defects to degradation: A mechanistic understanding of degradation in perovskite solar cell devices and modules. *Adv. Energy Mater.* **10**, 1904054 (2020). doi:10.1002/aenm.201904054
55. F. Zhang, S. Y. Park, C. Yao, H. Lu, S. P. Dunfield, C. Xiao, S. Uličná, X. Zhao, L. Du Hill, X. Chen, X. Wang, L. E. Mundt, K. H. Stone, L. T. Schelhas, G. Teeter, S. Parkin, E. L. Ratcliff, Y. L. Loo, J. J. Berry, M. C. Beard, Y. Yan, B. W. Larson, K. Zhu, Metastable Dion-Jacobson 2D structure enables efficient and stable perovskite solar cells. *Science* **375**, 71–76 (2022). doi:10.1126/science.abj2637 Medline

ACKNOWLEDGMENTS

The authors thank Dr. E. Tsai's and Dr. R. Li's from Brookhaven National Laboratory for their assistance with X-ray scattering measurements. **Funding**: X-ray scattering measurements were conducted at the Center for Functional Nanomaterials (CFN) and the Complex Materials Scattering (CMS) beamline of the National Synchrotron Light Source II (NSLS-II), which both are U.S. DOE Office of Science Facilities, at Brookhaven National Laboratory under Contract No. DE-SC0012704. The authors acknowledge the use of Princeton's Imaging and Analysis Center, which is partially supported through the Princeton Center for Complex Materials (PCCM), a National Science Foundation (NSF)-MRSEC program (DMR-2011750). Y.-L.L. acknowledges support from the National Science Foundation, under grants DMR-1627453 and CMMI-1824674. F.G. acknowledges the Swedish Government Strategic Research Area in Materials Science on Functional Materials at Linköping University (Faculty Grant SFO-Mat-LiU No. 2009-00971). T.R.L. thanks the Julis Romo Rabinowitz Graduate Fellowship for funding. Q.C.B. thanks the Arnold and Mabel Beckman Foundation for supporting this work. **Author contributions:** Y.-L.L. directed and supervised the project. X.Z. conceived the idea, initialized the project, and contributed to films and devices fabrication and characterization. T.R.L. and Q.C.B. contributed to accelerated stability studies. T.J.L. and F.G. contributed to temperature-dependent conductivity studies. R.H. contributed to XRD refinements. G.C. and N.Y. contributed to device stack imaging. All authors contributed to discussions and to finalizing the manuscript. **Competing interests:** None declared. **Data and materials availability:** All data needed to evaluate the conclusions in the paper are present in the paper or the Supplementary Materials.

SUPPLEMENTARY MATERIALS

science.org/doi/10.1126/science.abn5679
Materials and Methods
Supplementary Text
Figs. S1 to S15
Table S1
References (*34*–*55*)

Submitted 5 December 2021; accepted 19 April 2022
Published online 16 June 2022
10.1126/science.abn5679

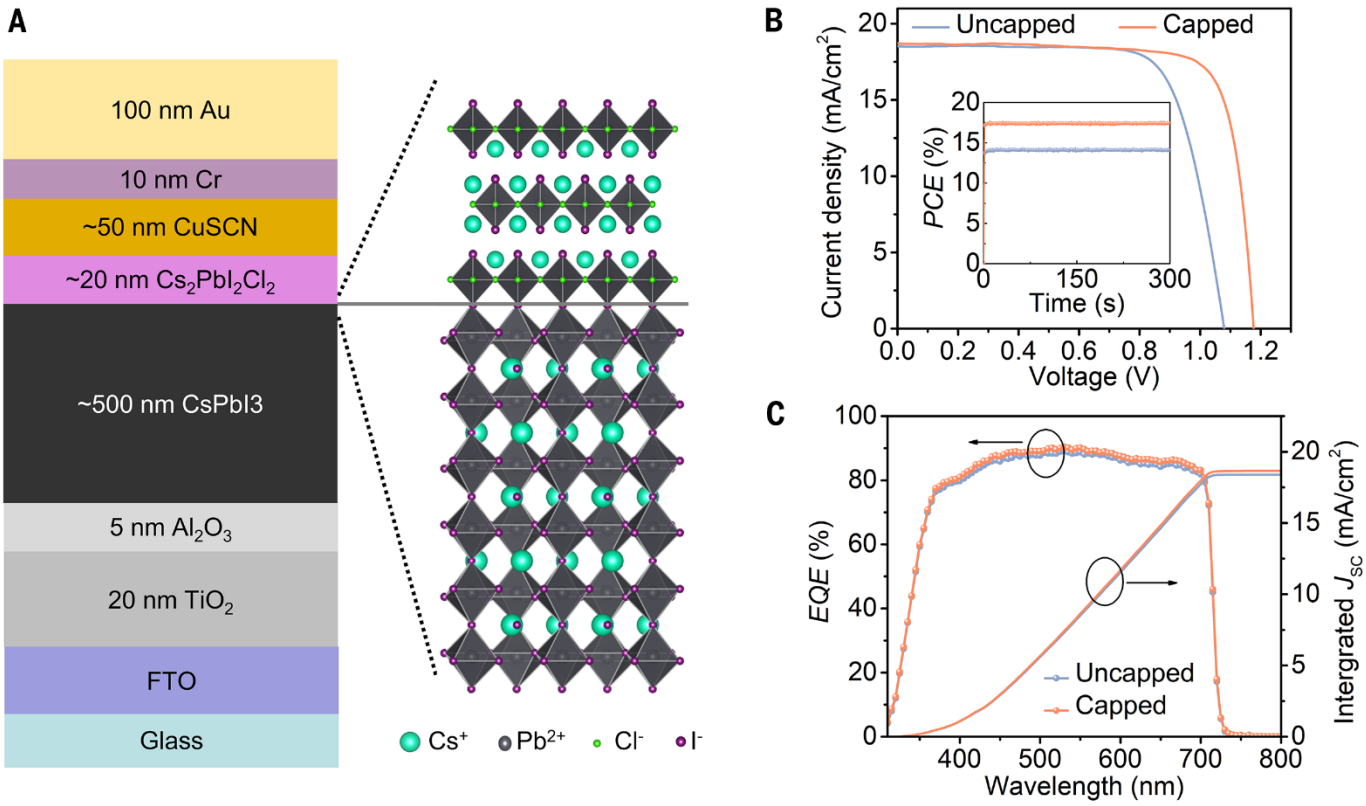

Fig. 1. Device structure and photovoltaic characterization. (**A**) Illustration of the capped device structure used in this work with a 2D $Cs_2PbI_2Cl_2$ layer atop the 3D perovskite active layer. (**B**) Current-density vs. voltage (*J-V*) characteristics under reverse voltage scan (inset: stabilized power output) and (**C**) external quantum efficiency (EQE) spectra and integrated J_{SC} of capped and uncapped champion solar cells.

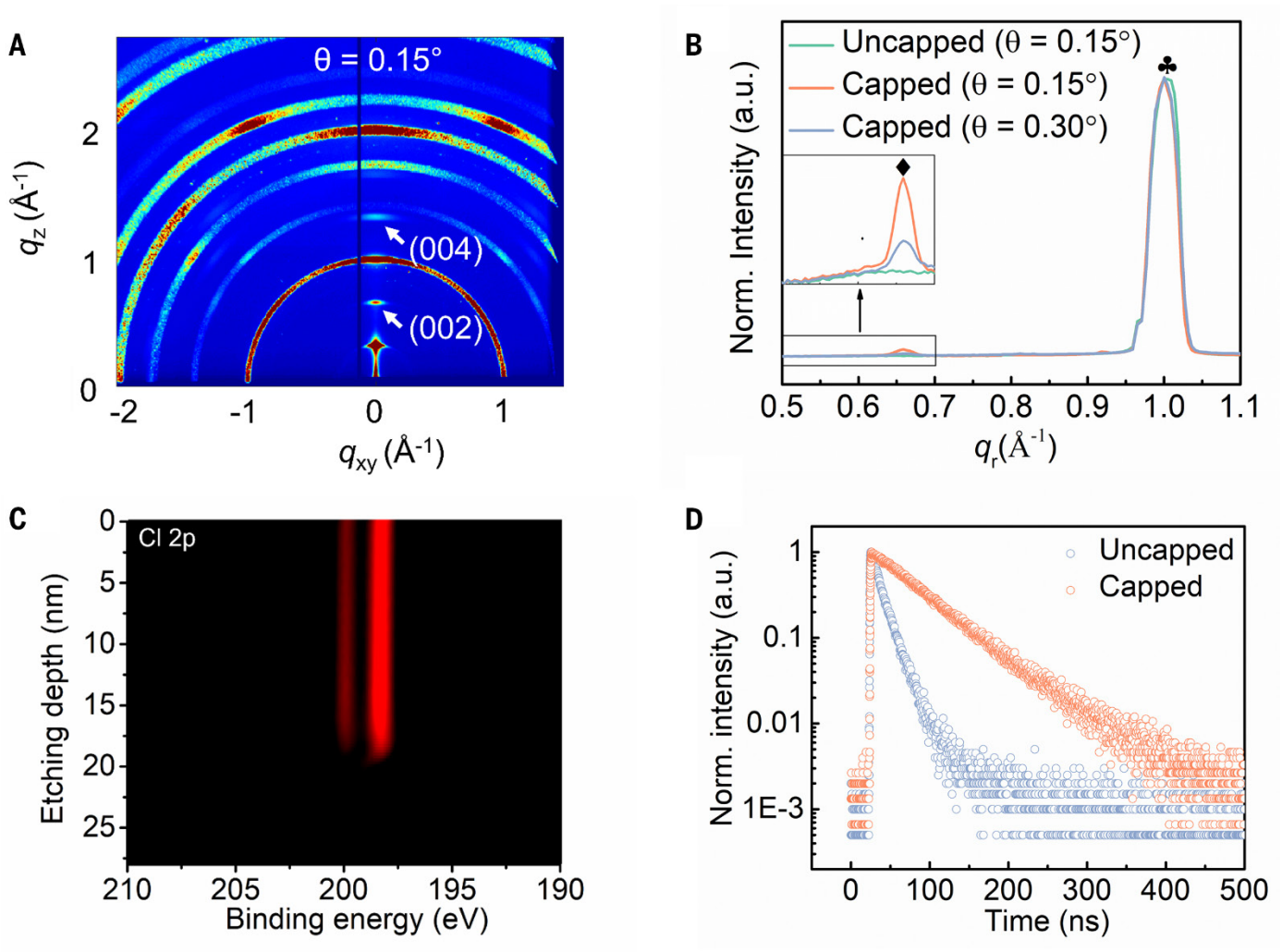

Fig. 2. Characterization of 2D perovskite capping layers. (**A**) GIWAXS patterns of a $Cs_2PbI_2Cl_2/CsPbI_3$ perovskite stack taken at a surface-sensitive incident angle of 0.15°. Characteristic reflections of $Cs_2PbI_2Cl_2$ are indicated. (**B**) Azimuthally-integrated GIWAXS traces collected on uncapped and capped samples at incident angles of θ = 0.15° (more surface-sensitive), and θ = 0.30° (less surface-sensitive). For reference, the critical angle is θ = 0.24°. The diamond indicates the (002) reflection of $Cs_2PbCl_2I_2$ while the clover indicates the (110) reflection of $CsPbI_3$. (**C**) XPS Cl 2p depth profiling of the $Cs_2PbI_2Cl_2/CsPbI_3$ stack. (**D**) Transient photoluminescence of capped and uncapped films on glass, excited from the film side.

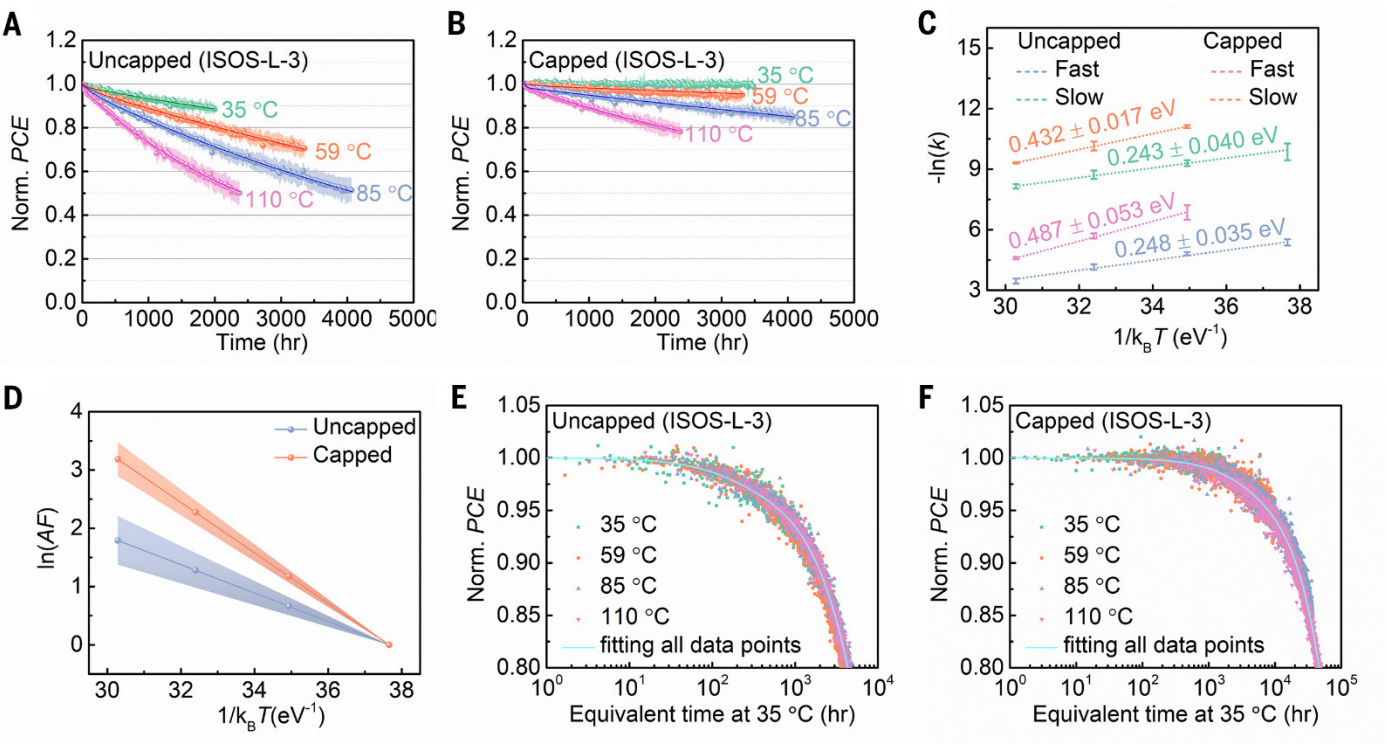

Fig. 3. Accelerated aging of PSCs operating at elevated temperatures. Operational stability of (**A**) uncapped and (**B**) capped PSCs operating at 35°, 59°, 85°, and 110°C, with standard deviation envelopes. The encapsulated devices were held at their MPP under constant full-spectrum simulated sunlight (power density ≈ 120 mW/cm^2) in (65 ± 26) % relative humidity air. Data points represent average *PCE* of three devices fabricated and tested under the same condition. The solid lines are bi-exponential fits to the data. (**C**) Natural logarithm of degradation rates (k_{fast} and k_{slow}) versus $1/k_BT$ obtained from biexponential fits to *PCEs* for uncapped and capped PSCs, where T is the aging temperature. Linear fits used to extract the activation energy (E_a) from each exponential are shown as the dash lines. Since the capped solar cells operating at 35°C did not show noticeable degradation over the time interval studied, their fitted values were not included. (**D**) Natural logarithm of AF versus $1/k_BT$ with the standard deviation represented by the shaded area around each line. Standard operating conditions for the AF calculation were defined as 1 sun illumination and T_{ref} = 35°C. (**E** and **F**) Normalized PCE of uncapped and capped PSCs plotted against the equivalent aging time at 35°C, defined as aging time (in units of hours) multiplied by the acceleration factor, for PSCs under all temperatures studied in this work.

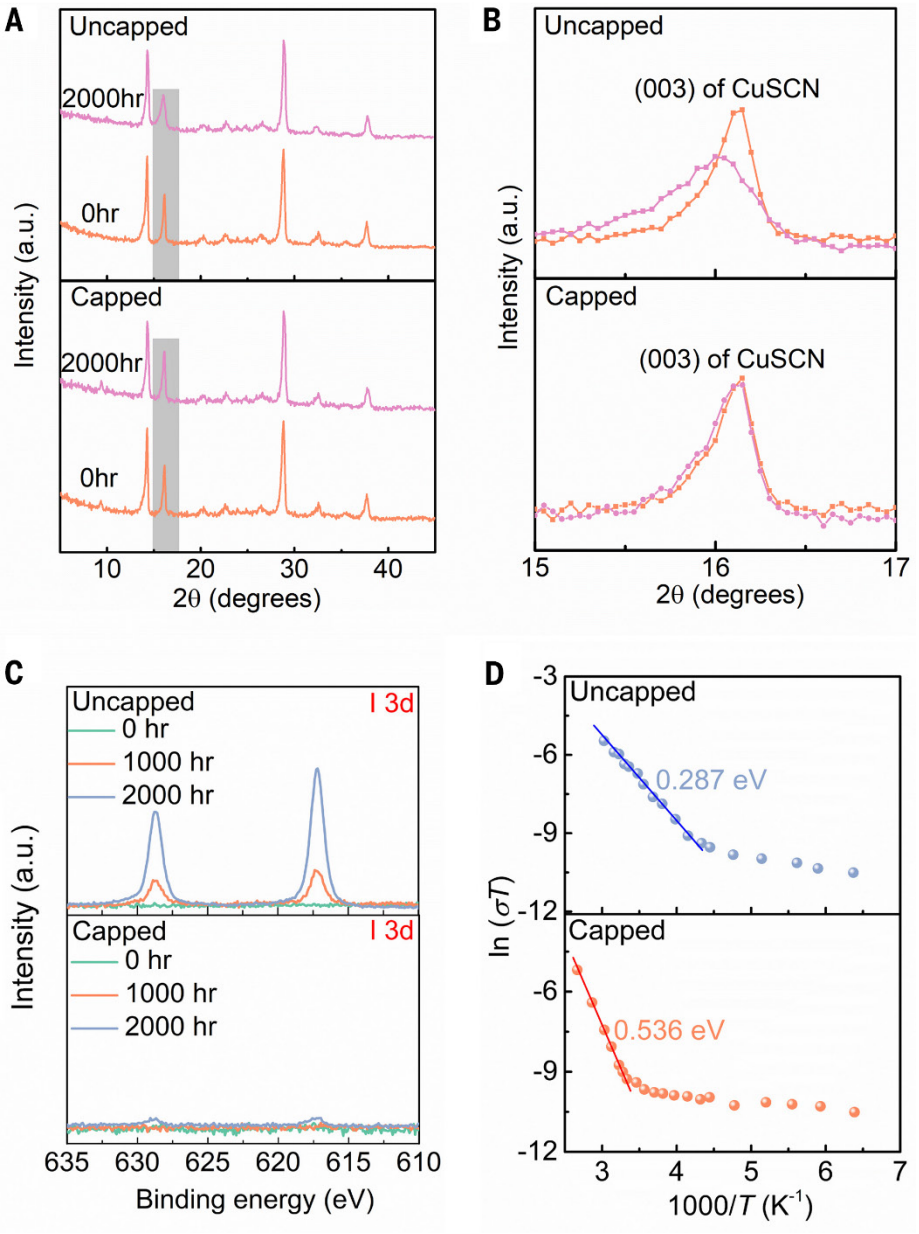

Fig. 4. Degradation/stabilization mechanism. (**A**) XRD traces of uncapped and capped PSCs before and after aging for 2000 hours, with (**B**) the region corresponding to CuSCN (003) diffraction magnified. (**C**) XPS I 3d spectra of the CuSCN surface in uncapped or capped PSCs with aging time on removal of the top electrode. For studies in Fig. 4a-c, full-stack, functional devices were sealed in N_2 and placed under full-sun illumination at 110°C for the specified time before the electrodes were peeled off prior to measurement. (**D**) Temperature-dependent conductivity (σ) of uncapped and capped films.

Accelerated aging of all-inorganic, interface-stabilized perovskite solar cells

Xiaoming ZhaoTianran LiuQuinn C. BurlingameTianjun LiuRudolph Holley IIIGuangming ChengNan YaoFeng GaoYueh-Lin Loo

Science, **Ahead of Print** • DOI: 10.1126/science.abn5679